




Magnetic properties of melt-spun MM–Fe–B ribbons with different wheel speeds and mischmetal contents

Xue-Feng Zhang, Wen-Kai Zhang, Yong-Feng Li* , Yan-Li Liu,
Zhu-Bai Li, Qiang Ma, Meng-Fei Shi, Fei Liu

Received: 17 March 2015 / Revised: 22 July 2015 / Accepted: 24 April 2016 / Published online: 6 June 2016
© The Nonferrous Metals Society of China and Springer-Verlag Berlin Heidelberg 2016

Abstract In this study, the effect of wheel speed and mischmetal (MM) content on the magnetic properties of MMFeB ribbons was investigated. The samples were prepared via direct solidification technique. The nominal composition of the alloy ingots is $\text{MM}_x\text{Fe}_{92-x}\text{B}_8$ with x varying from 9 to 15 in steps of 2. Experimental results show the overall magnetic properties of the ribbons. Analysis of the results shows that the magnetic properties first improve and then degrade with the wheel speed and MM content increasing. Increase in MM content leads to better formation of crystal texture in the ribbons, indicating that the α -Fe phase might undermine the formation of crystal texture. Magnetic properties results show that the coercivity of the ribbons rises with an appropriate increase in both MM content and wheel speed during melt-spun process. The strongest magnetic properties of the ribbons (remanence of $M_r = 0.72$ T, intrinsic coercivity of $H_{cj} = 352.58$ kA·m⁻¹, and maximum energy product of $(BH)_{\max} = 72.14$ kJ·m⁻³) are obtained for compositions where $x = 13$ and a wheel speed of $v = 20$ m·s⁻¹.

Keywords Mischmetal; MMFeB; Magnetic properties; Melt spun

1 Introduction

Since its discovery in 1983 [1], sintered NdFeB permanent magnets have become the fastest growing and most widely used rare earth permanent magnetic material because of its excellent comprehensive magnetic performance. This performance continues to improve through advancements in preparative techniques and composition optimization [2–5]. At present, the need of sintered rare earth permanent magnets material has been increasing in the market [6]. In recent years, raw materials such as the metals Nd and Pr used in preparing NdFeB materials have become scarcer, which results in a sharp rise in the price of materials for sintered NdFeB permanent magnets and creates enormous challenges for the sintered NdFeB industry. Because of the cost pressure of PrNd and Dy metals, the issue on substitution of PrNd by mischmetal (MM) alloys attracted renewed attention [7] and another issue is that both Nd and Pr are extracted from mixed accretive rare earth mines, which are typically also rich in La and Ce [8, 9], and the cost of separating the rare earths is very high. On the other hand, La, Ce, Pr, and Nd are all 4f atom elements with a hexagonal close-packed (hcp) structure, so they can form chemical compounds of $\text{MM}_2\text{Fe}_{14}\text{B}$ with MM, Fe, and B [10]. Furthermore, La and Ce are effective in refining the grain size of these ribbons [11], and MMFeB is possible to be a potential nanocomposite magnetic material [12]. Therefore, it is possible to adjust the components used to create rare earth magnets so that they can better meet the available resource conditions in order to reduce costs and optimize resources [13]. In previous work, the common mixed rare earth metal MM which consists of large amounts of La and Ce and a small amount of Pr and Nd was used to prepare MM–Fe–B melt-spun ribbons.

X.-F. Zhang, W.-K. Zhang, Y.-F. Li*, Y.-L. Liu, Z.-B. Li,
Q. Ma, M.-F. Shi, F. Liu
Key Laboratory of Integrated Exploitation of Bayan Obo Multi-
Metal Resources, Inner Mongolia University of Science and
Technology, Baotou 014010, China
e-mail: wuleng@126.com

X.-F. Zhang, W.-K. Zhang, Y.-F. Li, Y.-L. Liu, Q. Ma,
M.-F. Shi, F. Liu
Schools of Mathematics, Physics and Biological Engineering,
Inner Mongolia University of Science and Technology,
Baotou 014010, China

In this paper, it is focused on how MM content (x) and quenching wheel speed (v) influence the microstructure and magnetic properties of the material, with the purpose of developing better magnetic properties in MMFeB magnets.

2 Experimental

In this experiment, MM is a very common mischmetal from Bayan Obo mine in Baotou, China, and it consists of La 28.63 wt%, Ce 50.13 wt%, Pr 4.81 wt%, Nd 16.38 wt%, and a few other impurities. Alloy ingots with a nominal composition of $\text{MM}_x\text{Fe}_{92-x}\text{B}_8$ ($x = 9, 11, 13, 15$) were prepared using a high-frequency melting furnace with MM, Fe, and FeB components under high-purity Ar atmosphere. The ingots were melted three times and thermally treated for 120 min to ensure homogeneity of the ingots. The arc-melt ingots were broken into small pieces and crushed into quartz tubes, and then melt-spun onto a copper wheel in argon atmosphere under different wheel speeds of 10, 15, 20, 25, 30, 40, and 50 $\text{m}\cdot\text{s}^{-1}$. The phases and grain sizes of the samples were characterized using X-ray diffraction (XRD, D8 ADVANCE) with Cu $K\alpha$ radiation. The magnetic hysteresis loops of the ribbons were measured using a vibrating sample magnetometer (VSM, Quantum Design VersaLab) with an applied field up to 3 T. The microstructure of the $\text{MM}_{13}\text{Fe}_{79}\text{B}_8$ alloy ingots was characterized by scanning electron microscope (SEM, QUANTA 400) equipped with energy-dispersive spectroscopy (EDS).

3 Results and discussion

3.1 Structure and magnetic properties of melt-spun ribbons at different wheel speeds

Figure 1 shows the XRD patterns of melt-spun ribbons with different compositions at wheel speeds of 10, 15, 20, 25, 30, 40, and 50 $\text{m}\cdot\text{s}^{-1}$. As shown, the diffraction peak of the α -Fe phase disappears and the peak intensity of $\text{MM}_2\text{Fe}_{14}\text{B}$ gradually strengthens as the MM content increases, which indicates that the number of $\text{MM}_2\text{Fe}_{14}\text{B}$ phases in the sample increases as MM content increases. In addition, it is obvious that the diffraction pattern of the ribbons gradually widens with wheel speed increasing [14], suggesting that the average grain size decreases.

Table 1 shows the average grain size of the melt-spun ribbons with different compositions at wheel speeds of 10, 15, 20, 25, 30, 40, and 50 $\text{m}\cdot\text{s}^{-1}$. Zhao et al. [15] reported that the relationship between remanence enhancement and grain size can be written as:

$$M_r/M_s = 0.5 + 1.8\Delta_0/L \quad (1)$$

where M_r , M_s , Δ_0 , and L are the remanence, saturation magnetization, exchange length, and average grain size, respectively. At $x = 13$ and $v = 20 \text{ m}\cdot\text{s}^{-1}$, the ribbons have properties of $M_s = 1.23 \text{ T}$, $M_r = 0.72 \text{ T}$, and $\Delta_0 = 4/\pi$. The result of M_r/M_s is 0.585 and $0.5 + 1.8\Delta_0/L$ is 0.548, which are in good agreement with the model of remanence enhancement.

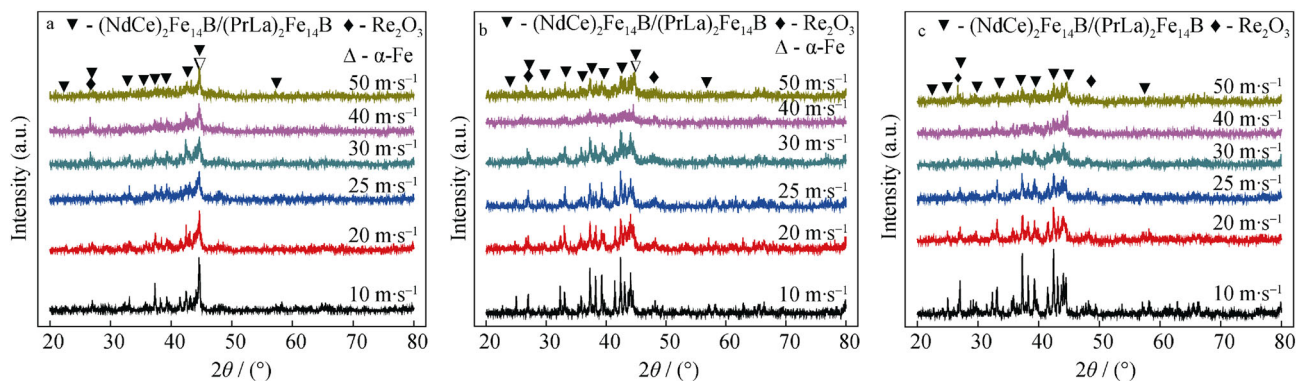


Fig. 1 XRD patterns of $\text{MM}_x\text{Fe}_{92-x}\text{B}_8$ melt-spun ribbons under different wheel speeds: **a** $x = 9$, **b** $x = 11$, and **c** $x = 13$

Table 1 Average grain size of $\text{MM}_x\text{Fe}_{92-x}\text{B}_8$ ($x = 9, 11, 13, 15$) melt-spun ribbons at wheel speeds of 10, 20, 25, 30, 40, and 50 $\text{m}\cdot\text{s}^{-1}$ (nm)

$\text{MM}_x\text{Fe}_{92-x}\text{B}_8$	10 $\text{m}\cdot\text{s}^{-1}$	15 $\text{m}\cdot\text{s}^{-1}$	20 $\text{m}\cdot\text{s}^{-1}$	25 $\text{m}\cdot\text{s}^{-1}$	30 $\text{m}\cdot\text{s}^{-1}$	40 $\text{m}\cdot\text{s}^{-1}$	50 $\text{m}\cdot\text{s}^{-1}$
$x = 9$	61.6	57.9	50.9	38.1	32.1	20.9	10.5
$x = 11$	59.2	55.2	50.2	39.5	30.9	23.8	9.6
$x = 13$	60.4	57.1	49.1	39.4	31.8	230.0	11.5
$x = 15$	59.8	55.7	49.9	38.4	29.3	21.7	10.2

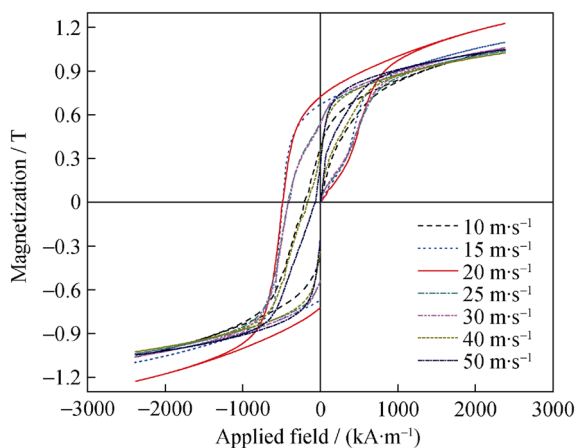


Fig. 2 Hysteresis loop of $\text{MM}_{13}\text{Fe}_{79}\text{B}_8$ melt-spun ribbons produced under different wheel speeds

Figure 2 presents the magnetic hysteresis loops of the $\text{MM}_{13}\text{Fe}_{79}\text{B}_8$ melted ribbons melt spun at wheel speeds of 10, 15, 20, 25, 30, 40, and 50 $\text{m}\cdot\text{s}^{-1}$. Note that the squareness of the hysteresis loop is poor at very low and very high wheel speeds, while the demagnetization curves at wheel speeds of 15 and 20 $\text{m}\cdot\text{s}^{-1}$ are very smooth. Figure 3 shows the variation in maximum M_r , coercivity (H_{cj}), and maximum energy product ($(BH)_{\max}$) values as a function of wheel speed for the $\text{MM}_{13}\text{Fe}_{79}\text{B}_8$ melt-spun ribbons. All of the ribbons' magnetic properties (M_r , H_{cj} ,

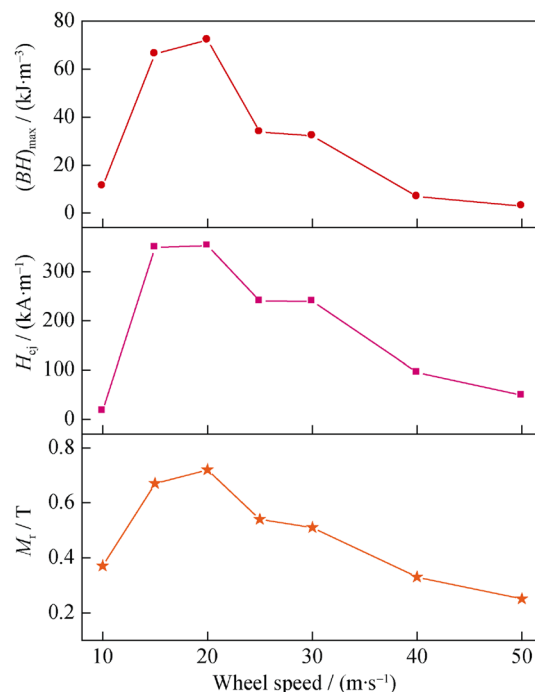


Fig. 3 Variation in maximum values for M_r , H_{cj} , and $(BH)_{\max}$ of $\text{MM}_{13}\text{Fe}_{79}\text{B}_8$ melt-spun ribbons as a function of wheel speed

and $(BH)_{\max}$) first increase as the wheel speed increases up to 20 $\text{m}\cdot\text{s}^{-1}$ and then decrease. The best magnetic properties are obtained at a wheel speed of 20 $\text{m}\cdot\text{s}^{-1}$, achieving

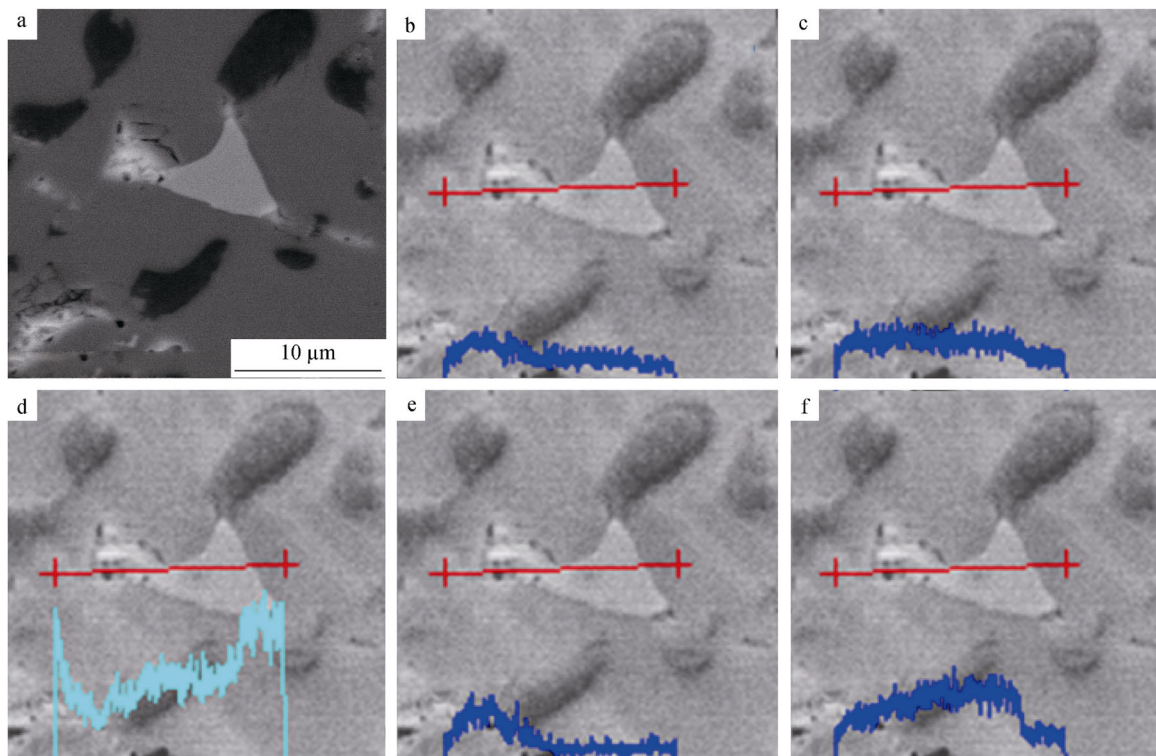


Fig. 4 SEM-BSE image of $\text{MM}_{13}\text{Fe}_{79}\text{B}_8$ alloy ingot and elemental EDS line scan maps across matrix phase and rare earth phase regions: **a** SEM-BSE image, **b** Pr, **c** Nd, **d** Fe, **e** La, and **f** Ce

an M_r value of 0.72 T, an H_{cj} value of 352.58 kA·m⁻¹, and a $(BH)_{max}$ value of 72.14 kJ·m⁻³.

3.2 Rare earth and Fe distribution in melt-spun ribbons

From the backscattered electron (BSE) map of the MM₁₃Fe₇₉B₈ ingot in Fig. 4, the compositional variation that occurs across the region in the EDS intensity profiles can be clearly seen. The scanned region can be divided into a Re-rich phase in which Fe content is low, and a matrix phase in which Fe content is high. This suggests that Ce has a stronger affinity with Nd, while La has a stronger affinity with Pr. Thus, La, Pr, Fe, and B preferentially form (PrLa)₂Fe₁₄B as a metallic phase. Furthermore, when Pr, Nd, and La contents are lower, Ce content is spiked, indicating that the excess Ce, Fe, and B form Ce₂Fe₁₄B phase in these ribbons instead.

3.3 Magnetic properties of melt-spun ribbons with different MM contents

The magnetic properties of MM_xFe_{92-x}B₈ ($x = 9, 11, 13, 15$) melt-spun ribbons prepared at wheel speeds of 10, 15, 20, 25, 30, 40, and 50 m·s⁻¹ were measured by VSM, with the results shown in Table 2. The data in Table 2 show that the magnetic properties of the ribbons all first increase as the MM content increases at wheel speeds of 10, 15, 20, 25, 30, 40, and 50 m·s⁻¹. This result indicates that increasing the MM content leads to the production of a harder magnetic phase MM₂Fe₁₄B alloy with a corresponding decrease in the α -Fe phase, resulting in the enhancement of the remanence and coercivity of the ribbons. Therefore, the remanence, coercivity, and maximum energy product all correspondingly increase.

Furthermore, it can be seen that all of the magnetic properties (M_r , H_{cj} , and $(BH)_{max}$) also first increase as the wheel speed increases for a given composition. In this scenario, the average grain size of the ribbon decreases as the wheel speed increases, and this gradually enhances the coercivity of the ribbon. Therefore, the coercivity and the maximum energy product increase together. However, it is worth noting that the coercivity of the ribbons drops precipitously beyond a wheel speed of 20 m·s⁻¹. Meanwhile, for the ribbons with the same composition, the relative intensity and the quantity of diffraction peaks for MM₂Fe₁₄B phase decrease with wheel speed increasing, indicating that the amount of MM₂Fe₁₄B phase decreases and that of amorphous increases with wheel speed increasing [16].

Table 2 Magnetic properties of MM_xFe_{92-x}B₈ ($x = 9, 11, 13, 15$) melt-spun ribbons with different wheel speeds (v) and MM content (x)

MM _x Fe _{92-x} B ₈	$v/(m \cdot s^{-1})$	M_r/T	$H_{cj}/(kA \cdot m^{-1})$	$(BH)_{max}/(kJ \cdot m^{-3})$
$x = 9$	10	0.26	60.59	3.43
	15	0.50	105.43	14.66
	20	0.52	140.52	18.45
	25	0.38	107.64	8.14
	30	0.31	67.04	4.87
	40	0.25	55.44	2.88
	50	0.14	30.63	0.20
$x = 11$	10	0.17	41.89	1.33
	15	0.49	118.34	13.48
	20	0.51	151.29	21.52
	25	0.41	117.32	13.37
	30	0.38	85.57	7.30
	40	0.30	55.44	3.57
	50	0.27	48.99	2.32
$x = 13$	10	0.37	17.32	11.21
	15	0.67	349.36	66.36
	20	0.72	352.58	72.14
	25	0.54	240.37	33.84
	30	0.51	239.80	32.22
	40	0.33	95.40	6.87
	50	0.25	49.01	2.91
$x = 15$	10	0.50	203.02	25.33
	15	0.51	265.55	38.28
	20	0.55	316.18	44.21
	25	0.50	237.69	28.01
	30	0.46	212.50	22.63
	40	0.45	207.48	21.57
	50	0.45	188.07	19.56

4 Conclusion

MM_xFe_{92-x}B₈ ($x = 9, 11, 13, 15$) magnetic ribbons were prepared by direct solidification, and the effect of MM content and wheel speed on the microstructure and the magnetic properties of the melt-spun ribbons was investigated. X-ray analysis shows that increasing MM content and wheel speed cause the α -Fe phase to disappear and the peak intensity of the MM₂Fe₁₄B phase to gradually strengthen, indicating that increasing MM content leads to a beneficial formation of the MM₂Fe₁₄B phase in the ribbon. VSM results show that M_r , H_{cj} , and $(BH)_{max}$ of the optimally processed MM_xFe_{92-x}B₈ ribbons first increase

with the increase in wheel speed, reaching maximum values at $v = 20 \text{ m}\cdot\text{s}^{-1}$, and then decrease with further increase in wheel speed. The results also show that the magnetic properties of the ribbons first increase with MM content increasing, reaching their maximum values at $x = 13$. Beyond this MM content, however, these properties decrease. In conclusion, it is able to produce melt-spun ribbons with excellent magnetic properties: $M_s = 1.23 \text{ T}$, $M_r = 0.72 \text{ T}$, $H_{cj} = 352.58 \text{ kA}\cdot\text{m}^{-1}$, and $(BH)_{\max} = 72.14 \text{ kJ}\cdot\text{m}^{-3}$, using an MM content of $x = 13$ (i.e., $\text{MM}_{13}\text{Fe}_{79}\text{B}_8$) and a wheel speed $v = 20 \text{ m}\cdot\text{s}^{-1}$.

Acknowledgments This work was financially supported by the National Natural Science Foundation of China (Nos. 51461033, 51571126, 51541105, and 11547032), the Inner Mongolia Innovative Research Team (No. 3400102), the Inner Mongolia Science Foundation (No. 2013MS0110), the Provincial Major Science and Technology Project of Inner Mongolia (No. 2009J1006), the Baotou Major Research Project Special for Rare Earth (No. 2012R1006), and the Inner Mongolia University of Science and Technology Innovation Fund.

References

- [1] Sagawa M, Fujimura S, Togawa N, Yamamoto H, Matsuura Y. New material for permanent magnets on a base of Nd and Fe. *J Appl Phys*. 1984;55(6):2083.
- [2] Yu LQ, Zhang J, Hu SQ, Han ZD, Yan M. Production for high thermal stability NdFeB magnets. *Magn Magn Mater*. 2008; 320(8):1427.
- [3] Hu ZH, Zhu MG, Li W, Lian FZ. Effect of Nb on the coercivity and impact toughness of sintered Nd–Fe–B magnets. *Magn Magn Mater*. 2008;320(3/4):96.
- [4] Li WF, Ohkubo T, Hono K. Effect of post-sinter annealing on the coercivity and microstructure of Nd–Fe–B permanent magnets. *Acta Mater*. 2009;57(5):1337.
- [5] Tang J, Yang LR, Zhang L, Wei CF, Mei Y, Wen YG. Succession law of Nd–Fe–B alloys with different coercivities. *Rare Met*. 2015;34(9):657.
- [6] Zhou SZ, Dong QF. *Super Permanent Magnets: Rare Earth Permanent Magnetic Material*. Beijing: Metallurgical Industry Press; 2004. 282.
- [7] Niu E, Chen ZA, Chen GA, Zhao YG, Zhang J, Rao XL, Hu BP, Wang ZX. Achievement of high coercivity in sintered R–Fe–B magnets based on misch-metal by dual alloy method. *J Appl Phys*. 2014;115(113912):1.
- [8] Guan LB, Niu JJ, Hao SZ, Wang JZ, Ma JH, An LJ, Li QY. Technical study of RE–Fe–B magnet preparation using mixture rare earth. *Mater China*. 2009;28(3):51.
- [9] Song HD, Chen PL. *Permanent Magnets Materials and Application*. Beijing: Metallurgical Industry Press; 1984. 7.
- [10] Zhou SZ, Dong QF, Gao XX. *Sintered NdFeB Rare Earth Permanent Magnet Materials and Technology*. Beijing: Metallurgical Industry Press; 2011. 65.
- [11] Chang WC, Wu SH, Ma BM, Bounds CO. The effects of La-substitution on the microstructure and magnetic properties of nanocomposite NdFeB melt spun ribbons. *Magn Magn Mater*. 1997;167(96):65.
- [12] Qiu J, Li SD, Liu MM, Wu JP, Hu Y, Cai XL, Lin JH, Wang LL. Effect of wheel speed on the microstructure and magnetic properties of melt-spun $(\text{Nd}_{0.75}\text{Dy}_{0.25})_{10.5}\text{Zr}_2\text{Fe}_{82}\text{B}_{5.5}$ ribbons. *Adv Mater Res*. 2012;569(1):23.
- [13] Wu SJ, Bao XQ, Xiang DL, Zhu J, Gao XX. Microstructure and magnetic properties of (Nd, Pr, Ce)–Fe–B magnets. *J Univ Sci Technol Beijing*. 2013;35(6):778.
- [14] Wang L, Chen JW, Yue M, Liu RM, Liu WQ, Zhang DT, Zhang JX, Zhang PY, Ge HL. Crystallographic alignment and magnetic anisotropy in melt-spun Nd–Fe–B/ α -Fe composite ribbons with different neodymium contents. *J Rare Earths*. 2011;29(5):471.
- [15] Zhao GP, Ong CK, Feng YP, Lim SH, Ding J. Remanence enhancement of single-phased isotropic nanostructured permanent magnets. *Magn Magn Mater*. 1999;192(543/552):551.
- [16] Bao XQ, Guo XY, Guo JC, Gao XX. Effect of Ga addition on the magnetic properties and microstructure of nanocrystalline $\text{Nd}_{12.3}\text{Fe}_{81.7}\text{B}_{6.0}$ ribbons. *Rare Met*. 2011;30(5):448.